J. Fluid Mech. (1977), *vol.* 79, *part* 2, *pp.* 231–256
Printed in Great Britain

Experimental determination of the main features of the viscous flow in the wake of a circular cylinder in uniform translation. Part 1. Steady flow

By MADELEINE COUTANCEAU AND ROGER BOUARD

Laboratoire de Mécanique des Fluides, Université de Poitiers, France

(Received 24 May 1976)

A visualization method is used to obtain the main features of the hydrodynamic field for flow past a circular cylinder moving at a uniform speed in a direction perpendicular to its generating lines in a tank filled with a viscous liquid. Photographs are presented to show the particular fineness of the experimental technique. More especially, the closed wake and the velocity distribution behind the obstacle are investigated; the changes in the geometrical parameters describing the eddies with Reynolds number ($5 < Re < 40$) and with the ratio λ between the diameters of the cylinder and tank are given. A comparison with existing numerical and experimental results is presented and some remarks are made about the calculation techniques proposed up to the present. The limits of the Reynolds-number range for which the twin vortices exist and adhere stably to the cylinder are determined.

1. Introduction

The determination of the plane viscous flow around a circular cylinder moving at a constant speed in a fluid previously at rest or, which is equivalent, around one at rest in a uniform velocity field is a fundamental problem because all difficulties which arise in it are amplified for obstacles of other shapes. Its field of application is then very large, being basic to the calculation of more complex flows. Furthermore, in the range of 'intermediate' Reynolds numbers, it has been the subject of numerous theoretical and, above all, numerical studies which have been developed over the last ten years with the general use of electronic computers. These studies have attempted to obtain approximate solutions that represent the real flow as exactly as possible. They essentially differ from one another in the calculation method, which may be analytical (matched Stokes and Oseen asymptotic expansions, for instance), semi-analytical (search for a solution in the form of series expansions by using, explicitly or not, the principles of series truncation) or numerical (finite-difference scheme), and in the expression of the boundary conditions.

For an unbounded flow field, the expression of the boundary conditions sets effectively a problem in numerical resolution, as the calculation field is necessarily

Author(s)	Reynolds numbers
Investigations from steady-state equations	
Thom (1928)	10
Thom (1933)	20
Homann (1936)	
Imai (1951)	
Kawaguti (1953)	40
Allen & Southwell (1955)	0, 1, 10, 10^2, 10^3
Lagerstrom & Cole (1955)	
Proudman & Pearson (1957)	
Kaplun (1957)	
Apelt (1958)	40, 44
Dennis & Shimshoni (1965)	0·01–∞
Underwood (1968)	0·4, 1·6, 6·4, 10
Takaisi (1969)	0·5–100
Takami & Keller (1969)	1, 2, 4, 6, 7, 10, 15, 20, 30, 40, 50, 60
Hamielec & Raal (1969)	1, 2, 4, 10, 15, 30, 50, 100, 500
Pruppacher, Le Clair & Hamielec (1970)	1–500
Dennis & Chang (1970)	5, 7, 10, 20, 40, 70, 100
Nieuwstadt & Keller (1973)	1, 7, 10, 20, 30, 40
Ta Phoc Loc (1975)	5, 20, 40, 60, 100, 120
Investigations from time-dependent equations	
Hirota & Miyakoda (1965)	40, 100
Kawaguti & Jain (1966)	10, 20, 30, 40, 50, 60, 100
Ingham, (1968)	40, 100
Jain & Rao (1969)	40, 60, 100, 200
Son & Hanratty (1969)	40, 200, 500
Thoman & Szewczyk (1969)	1, 30, 40, 200, 600, 4×10^4, 3×10^5
Collins & Dennis (1973)	5, 10, 40, 100, 200, 500, 10^3, 5×10^3, ∞

TABLE 1. Existing work.

bounded. To overcome this difficulty, some investigators use a conformal transformation that reduces the flow field to a bounded one, but this inevitably complicates the resolving of the equations; most others impose conditions at a finite distance from the obstacle which they think is sufficiently far away. These conditions express either the uniformity of the velocity field, or a matching with an Oseen flow (Imai's conditions) or with an irrotational flow, the obstacle being either in the middle part of the field, or in an eccentric upstream position.

Sometimes the calculations have been performed from simplified equations (boundary-layer equations), but more often from the Navier–Stokes equations. The methods used for this problem can be classified, from a general point of view, in two categories, according to whether they are limited to integration of steady-motion equations or whether they are concerned with the steady state as a limit of the solutions of the time-dependent equations; in this last case the calculations are of course more voluminous. To our knowledge, the main works in these two classes are those given in table 1 together with the Reynolds numbers at which they were done.

An analysis of the literature shows that, except for the length of the attached wake, the location of the separation point on the cylinder wall and the drag coefficient, rather little information exists concerning the detailed structure of the wake and its evolution against the Reynolds number.

Experimental work has received relatively less attention than numerical calculation. However, there have been several publications which can again be classified according to the methods used:

(i) *Visualization using dyed liquid.* Thom (1933), $3{\cdot}5 \leqslant Re \leqslant 10^3$.

(ii) *Visualization using bubbles.* Shair, Grove, Petersen & Acrivos (1963), $40 \leqslant Re \leqslant 150$; Grove, Shair, Petersen & Acrivos (1964), $30 \leqslant Re \leqslant 300$; Acrivos, Leal, Snowden & Pan (1968), $25 \leqslant Re \leqslant 177$.

(iii) *Visualization using solid particles.* Nisi & Porter (1923), $Re = 11{\cdot}6$, $24{\cdot}2$; Fage (1934), $17{\cdot}7 < Re < 170$; Taneda (1956*a*, 1964, 1965), $10^{-5} < Re < 2000$.

(iv) *Measurement with hot-wire anemometer.* Kovasznay (1949), $Re = 34$, 56; Nishioka (1973), $7 \leqslant Re \leqslant 80$; Nishioka & Sato (1974) $10 < Re < 80$.

(v) *Determination of the velocity gradients on the wall of the obstacle using an electrochemical technique.* Dimopoulos & Hanratty (1968), $60 < Re < 360$.

(vi) *Direct measurement of the pressures and of the forces.* Homann (1936), $Re = 100$; Tritton (1959), $0{\cdot}5 < Re < 100$.

It is to be noticed that in these experiments, except those of Taneda, the cylinder is not set in a stream of completely uniform velocity. On the other hand, whatever the method used, authors agree that their measurements become very inaccurate when the Reynolds number is less than 40, the velocity in the wake being then very low. Consequently in the experimental field also, the information is rather limited, particularly concerning features of the recirculating flow in the range of Reynolds numbers between the 'separation number' and the 'critical number' from which the wake begins to be asymmetrical. This is the reason why we think that we can provide a valid contribution in this difficult field using a method of velocity measurement from visualization photographs of fine enough definition, a method which we have previously developed and which has been shown to be accurate enough to determine the main features of the flow around a sphere, for Stokes flow and immediately beyond, with wall effects (Coutanceau 1968, 1972) or without wall effects (Payard & Coutanceau 1974).

2. Apparatus and preliminary tests

Experimental principle (figure 1)

The object of the experimental technique is to produce plane flow around a circular cylinder that is rising with a constant speed V_0 in a cylindrical tank which is of great diameter and which is filled with a liquid whose viscosity is suitable for obtaining the desired range of Reynolds numbers. The x axis of the tank is vertical, the z axis of the cylinder is horizontal and moves on a diametral plane of the tank. We take a photograph when the cylinder is about half-way up the tank so as to minimize the bottom effects and free-surface effects. The visualization so obtained allows us to measure velocities and to observe the flow structure. Wall influence is investigated by changing the ratio λ between the cylinder and tank diameters.

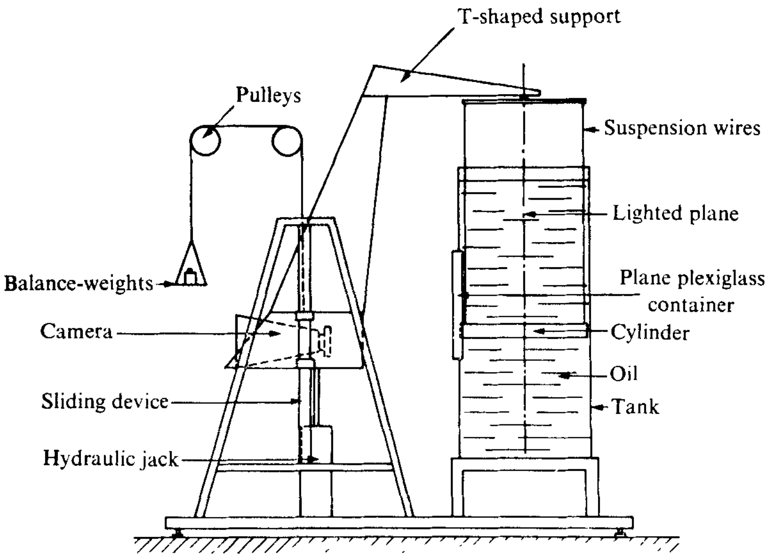

FIGURE 1. Schematic illustration of the apparatus.

Description of the apparatus

To refer the fluid motion to a frame that moves with the cylinder and thus obtain a steady flow, we couple the motion of the cylinder and the camera using a T-shaped support so that they go up together owing to a system of pulleys and balance-weights. The motion is guided by a sliding device with ball-bearings and is regularized by a hydraulic jack situated below the camera. The working speed V_0 of the cylinder is reached almost instantaneously (in less than $\frac{1}{100}$ s); it is measured by means of a photo-electric cell and an electronic chronometer.

Transparent Plexiglas cylinders were used; they are respectively 10 mm, 30 mm and 51 mm in diameter and slightly smaller in length than the tank diameter in order to reduce end effects: the maximum clearance is 5 mm. They are suspended at their extremities by two fine wires attached to the T-shaped support. The tank in which the cylinder moves is also made of transparent Plexiglas to allow visualization; it is 42 cm in internal diameter and 1 m in height. It is filled with a vaseline oil 'Marcol 80' which isvery stable in time and for which we have established the curve of kinematic viscosity against temperature with an accuracy better than 1 %; for instance it is 31·75 cS at 20 °C.

The fluid temperature is made uniform before every experiment: after steps have been taken to maintain the temperature of the experiment room as constant as possible, we improve the temperature uniformity of the fluid by stirring it with a screw driven by an electric motor. We then wait till the liquid has come completely to rest before conducting the experiment. A careful control shows that the temperature remains constant throughout the fluid within 0·1 °C for more than 1 h.

To compensate for the effects of the cylindrical diopter, we contrive to make the side of the tank that is in the field of the camera optically equivalent to a plane diopter by fixing on the tank wall a Plexiglas container filled with liquid the same as that contained in the tank or with a liquid of the same refractive index.

Visualization

The visualization method consists of illuminating by a sheet of intense light a meridian section of the tank, having suspended fine bright particles uniformly in the liquid, and then taking a photograph in the direction normal to the lighted plane.

The aluminium lamellas that are often used in other circumstances exhibit here inconvenient optical orientation phenomena (Bourot & Moreau 1949; Bourot, Coutanceau & Moreau 1962), and so we have replaced them by tiny magnesium cuttings 20 to 40 μm long and 4 to 5 μm thick. These cuttings, being complex in shape, radiate light in nearly all directions (instead of reflecting it in a preferential direction as plane lamellas would do, with the consequence that certain parts of their trajectories would then be invisible). The speed of these particles is low enough for the visualization made in these conditions not to raise a 'fidelity' problem.

The lighting is provided by a powerful arc-projector Breguet-Chartier (Chartier 1937) that works with a 80 V continuous tension and a 140 A current strength. A diaphragm limits the width of pencil rays to 2 cm. This pencil of rays is diaphragmed again before it enters the tank by an adjustable narrow slit of about 1 mm in breadth; the magnesium particles are intensely lit up. To take photographs, we use a camera 9×12 cm fitted with a lens of 135 mm in focal length and a variable aperture.

Technique for analysing photographs

During the time of exposure, a particle describes a trajectory whose length is proportional to the particle velocity. This length can be compared with a reference length that represents, taking into account the photographic magnification, the cylinder displacement during the exposure. To get good definition we adopt a magnification of 0·5. The reference length is obtained by superimposing on the photographic plate the trace formed by the image of a stationary bright point located in the lighted plane.

We measure the lengths of the dashes directly on the negative, mounting them on a stage placed beneath a binocular lens of several magnifying powers (between 4 and 25) which can be moved in two perpendicular directions by means of micrometer screws, thus allowing the displacements to be measured to $\frac{1}{100}$ mm.

The particle position is located by the co-ordinates (x, y) of the middle of the trace referred to the cylinder radius. Provided that some detailed corrections are made, especially a 'thickness correction' to account for halation in the sensitized film (Coutanceau 1971), we can obtain with this method, some meticulousness and patience a very good resolution of the velocity field with, in most of the flow, an inaccuracy less than 2%.

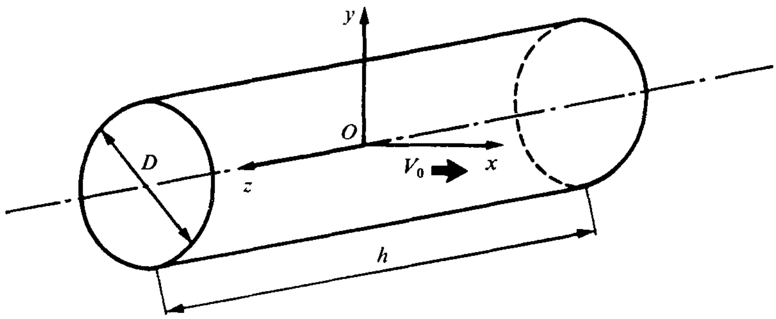

FIGURE 2. Co-ordinate system referred to the cylinder.

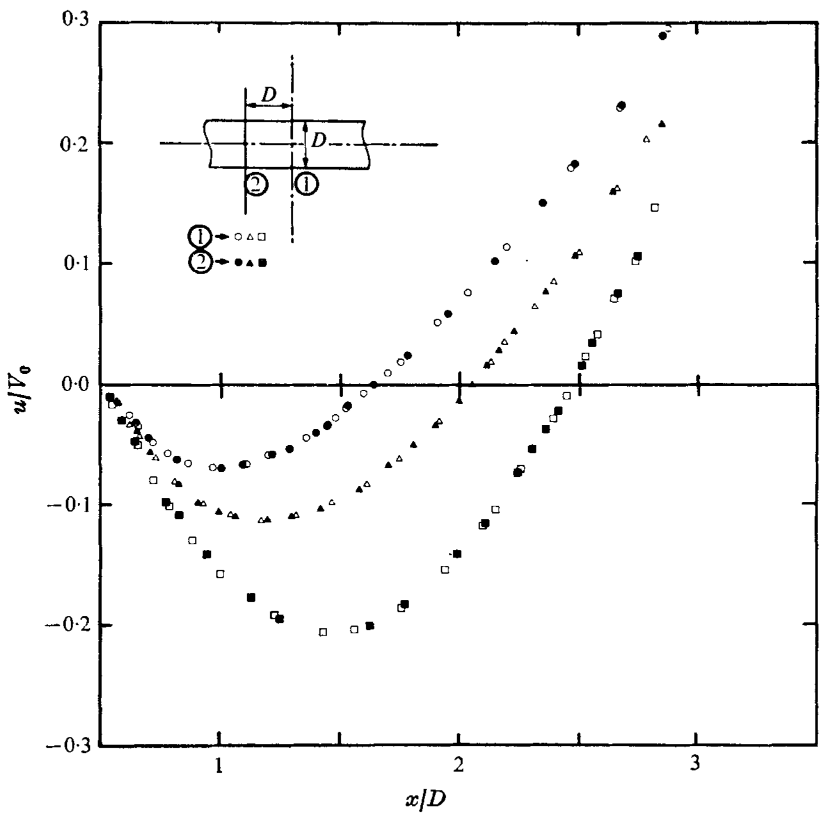

FIGURE 3. Velocity distribution on the rear flow axis at two cross-sections one cylinder diameter distant from each other, for $\lambda = 0{\cdot}12$. ●, ○, $Re = 29{\cdot}5$; ▲, △, $Re = 36{\cdot}6$; ■, □, $Re = 51{\cdot}7$.

Tests on the effects of the cylinder ends and on the establishment of the flow

Preliminary experiments have been carried out to check that the two-dimensional flow conditions are well realized. For this purpose, we took photographs of the flow in the meridian plane XOZ that contains the cylinder axis (figure 2). The corresponding visualizations show that the end effects are smaller if the cylinder length h is close to that of the tank diameter. Thus the clearance between the cylinder end and the tank wall was made as small as possible.

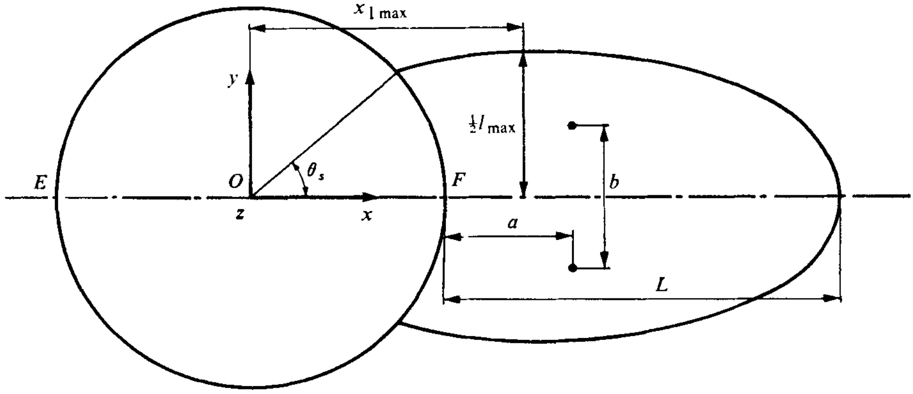

FIGURE 5. Geometrical parameters of the closed wake.

In these conditions, the experiments show that away from the end of the cylinder the end effects do not influence the measurement zone for a relatively large distance (about 15 cm in total length) on both sides of the median right section XOY (even in the most unfavourable case). We find, for instance, (i) that the velocities are, in practice, in right section planes (figure 7, plate 2). (ii) That the length of the wake attached to the cylinder is the same in a zone that covers about the half-length of the cylinder, i.e. 20 cm. The wake boundary appears clearly in, for example, figure 7; it is formed by the points of zero velocity. (iii) That the velocities in the different right section planes on the rear symmetry axis of the flow are the same, within the measurement accuracy, for Reynolds numbers regularly spaced in the range selected for experimentation, since the curves are superposed (figure 3).

Further, taking photographs after a greater period of time following the start of the cylinder verified that the flow is well established in the survey field.

3. Results and discussion

Flow-pattern presentation

Using the experimental technique just described and changing successively the ratio λ between the diameters of the cylinder and tank and the Reynolds number Re, we get and analyse a very great number of visualized flow patterns (more than 200 on the whole); for the most part, these have been taken along the cross-section plane XOY of the cylinder.

As as example, figure 4 (plate 1) shows the flow downstream of the cylinder for $Re = 24{\cdot}3$ and $\lambda = 0{\cdot}12$. Even for this relatively small value of the Reynolds number the closed wake region attached to the rear of the cylinder, usually called 'standing eddies' or 'twin vortices', appears very clearly. In particular, we see that the geometrical parameters of this region can be measured: the length L, the width l, the flow separation angle θ_S and the position of the vortex centres which can be located on the x and y axes by a and b (figure 5).

In this case, the axis of the camera is parallel to the cylinder generators; it is set behind the obstacle to allow visualization of all of the standing eddies.

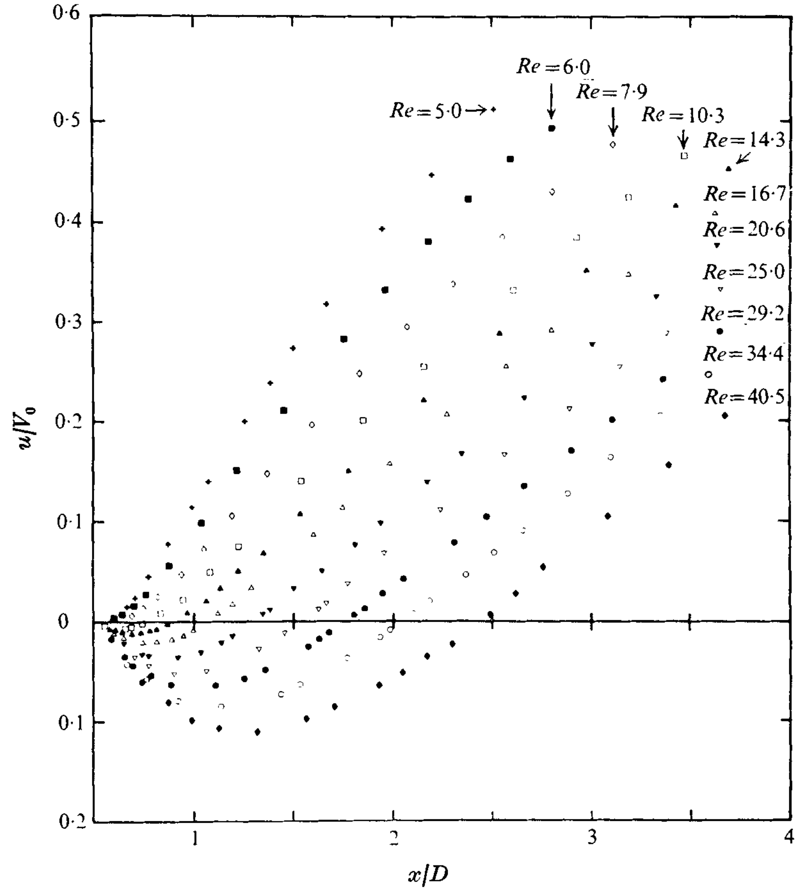

FIGURE 10. Velocity distribution on the rear flow axis when $\lambda = 0{\cdot}07$ for different *Re* values.

Optical and mask effects occur towards the direction of the upstream obstacle that we do not wish to visualize.

Thus, the very well-lighted white arc of the circle does not correspond to the real outline of the cylinder; the big dark circle in front is due to the mask effect produced by the end section which is in the camera direction and the two dark angles arise from a difference between the refractive indices of the liquid and cylinder: a total refraction phenomenon occurs along the opposite portions of the cylinder, i.e. in the cross-section XOY, along the arcs of circle located near the stagnation points E and F (figure 5). In fact, the cylinder is situated between the straight parallel lines which limit the outside of the dark angles.

Figure 6 (plate 2) shows, for steady flow and $\lambda = 0{\cdot}07$, the change in shape of the closed wake when the Reynolds number increases from 10·3 to 35·2: its length and width become more and more enlarged and the separation point on the cylinder moves upstream. For these *Re* values, it can be seen that the wake is steady and the vortices are symmetrical.

The effect of wall proximity, resulting in fact from the presence of the obstacle,

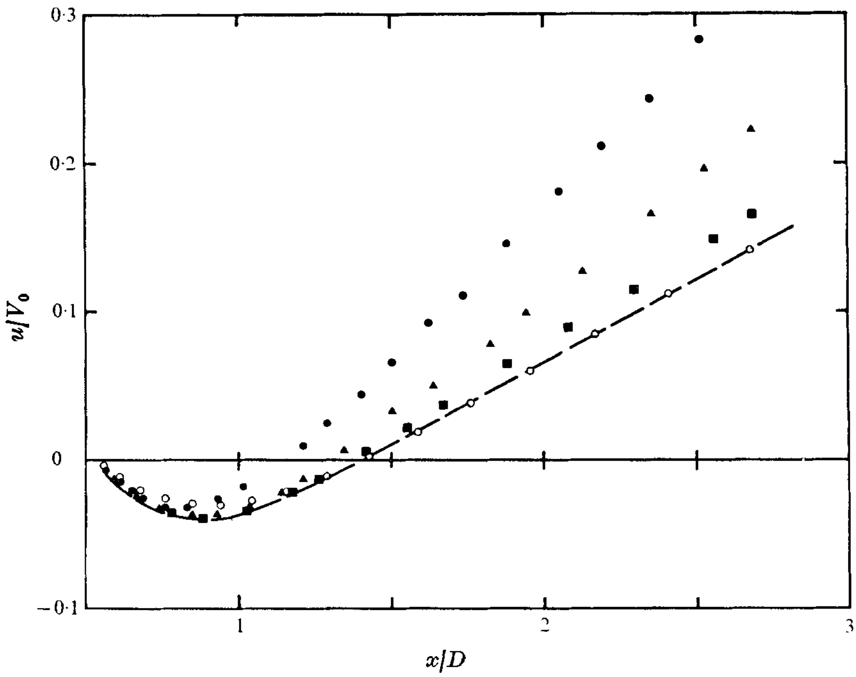

FIGURE 11. Velocity distribution on the flow axis behind the cylinder for $Re \simeq 20$ and for different λ values. Our experimental results: ●, $\lambda = 0{\cdot}12$, $Re = 19{\cdot}9$; ▲, $\lambda = 0{\cdot}07$, $Re = 20{\cdot}6$; ■, $\lambda = 0{\cdot}024$, $Re = 20{\cdot}1$; — —, $\lambda = 0$, $Re = 20$. Nieuwstadt & Keller's theoretical data (1973): ○, $\lambda = 0$, $Re = 20$.

which creates a flow-blockage effect, is shown in figure 9 (plate 3): for comparable *Re* the standing eddies are less developed when the diameter ratio is greater, i.e. when the wall is nearer. Then the relative inertia effect is reduced by the wall proximity. We have already shown this phenomenon in our study on the flow generated by a sphere which moves along the axis of a cylinder filled with a viscous liquid (Coutanceau 1971). For the smaller cylinder, i.e. when $\lambda = 0{\cdot}024$, our apparatus does not permit us to get *Re* values higher than 25. Figure 8 (plate 2) shows the flow when $\lambda = 0{\cdot}07$ and $Re = 40{\cdot}3$; the standing eddies have just become asymmetrical.

Velocity measurements

Analysing the photographs the way we have described, we measured the velocities in the flow field behind the cylinder, in particular on the flow axis. These results are illustrated graphically in figure 10 for $\lambda = 0{\cdot}07$ and different Reynolds number values ranging from 5 to 40·5. Similar curves have been plotted for $\lambda = 0{\cdot}024$ and 0·12. At this point we remark that these measurements, made for relatively small values of the diameter ratio λ, allow us to estimate by extrapolation the velocities and the other features of the case $\lambda = 0$, i.e. the case in which the tank is of infinite diameter.

The part of the curves below the x axis corresponds to returning flow in the wake region and thus shows the presence of eddies. For this Reynolds-number

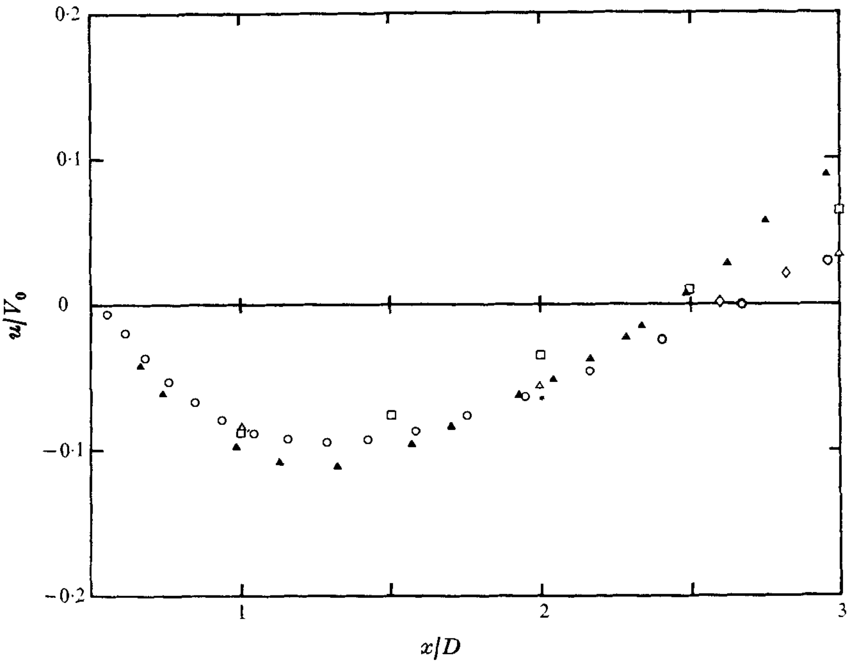

FIGURE 12. Velocity distribution on the flow axis behind the cylinder for $Re \simeq 40$ and for different λ values. Our experimental results: ▲, $\lambda = 0{\cdot}07$, $Re = 40{\cdot}5$. Theoretical data for $\lambda = 0$ and $Re = 40$: □, Kawaguti (1953); △, Apelt (1958); ○, Nieuwstadt & Keller (1973). Other experimental measurements: *, $Re = 34$, Kovasznay (1949); ◇, $Re = 40$, Nishioka & Sato (1974).

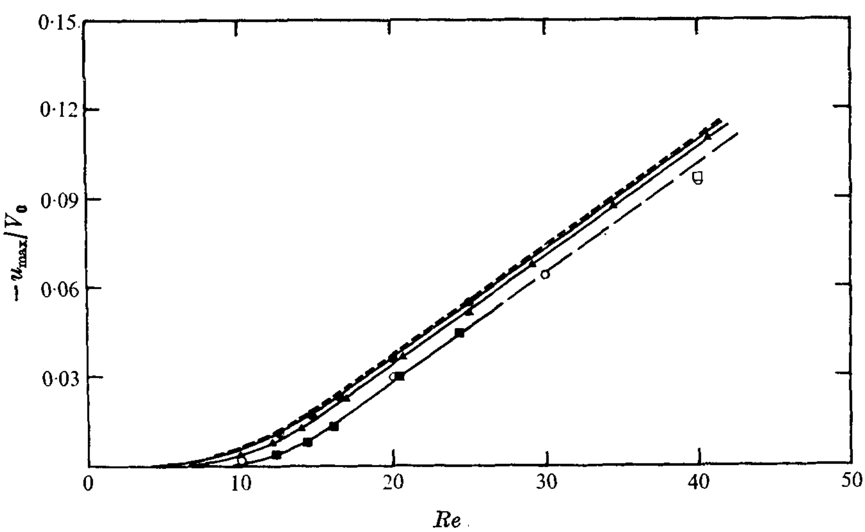

FIGURE 13. Evolution of the velocity maximum against Re on the rear flow axis in the closed wake of the cylinder. Present study: ■, $\lambda = 0{\cdot}12$; ▲, $\lambda = 0{\cdot}07$; ●, $\lambda = 0{\cdot}024$; ------, $\lambda = 0$. Theoretical data: □, Kawaguti (1953); ○, Nieuwstadt & Keller (1973).

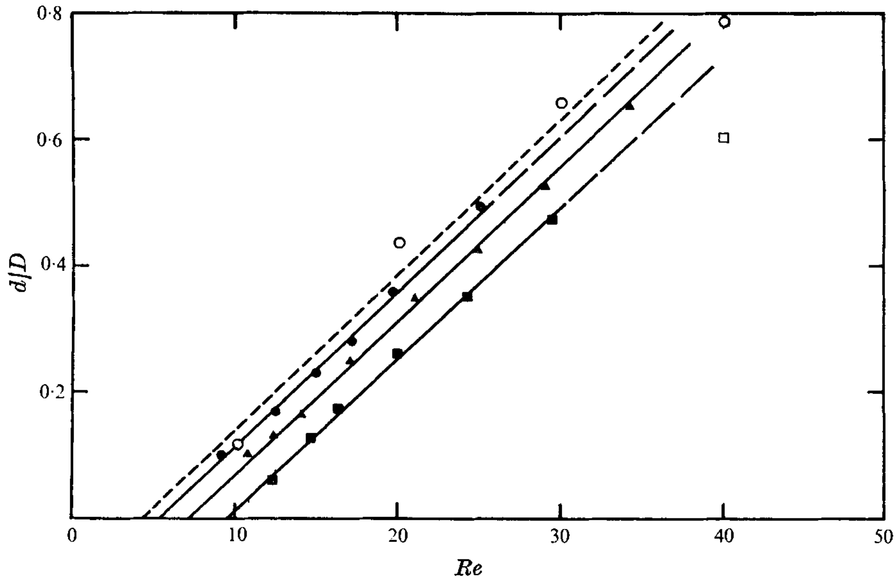

FIGURE 14. Location of the velocity maximum plotted against Re. Present study: ■, $\lambda = 0{\cdot}12$; ▲, $\lambda = 0{\cdot}07$; ●, $\lambda = 0{\cdot}024$; ------, $\lambda = 0$. Theoretical data: □, Kawaguti (1953); ○, Nieuwstadt & Keller (1973).

range, we see that the velocities in the vortices are very small. However, we have been able to measure them with reasonable accuracy, something not done until now by any other experimental investigator. As a matter of fact, the only measurements that have been made so far concern larger Re values ($Re > 40$). Yet, in the case where there is no wall effect and beyond $Re = 40$, the flow is unsteady and measuring becomes uneasy. That is the reason why some authors, such as Grove *et al.* (1964), artificially stabilized the wake, thus inevitably altering it. Consequently, any quantitative information on the flow development in the range of Reynolds numbers investigated here can be deduced from these experiments by extrapolation.

As in the experimental investigation, obvious difficulties arise in theoretical investigations: a very high accuracy is necessary for every step in the calculation process. Among the many quoted authors, only Kawaguti (1953), Apelt (1958) and Nieuwstadt & Keller (1973) have given some information about the velocity in the range of Re considered. As examples, their results and the results inferred from our experiments are compared in figures 11 and 12.

When standing eddies exist behind the cylinder, the velocity along the centreline of the wake, which is negative in the corresponding closed recirculating region, takes a maximum value u_{max} at a certain point P_{max} which we locate by its distance d from the rear stagnation point F. The values of u_{max} and of d are interesting parameters to characterize the flow structure in this region. So, their evolution with Re is given in figures 13 and 14 when $\lambda = 0{\cdot}024$, $0{\cdot}07$, $0{\cdot}12$. The extrapolated curve ($\lambda = 0$) and the numerical values deduced from the results of Kawaguti and Nieuwstadt & Keller have also been included.

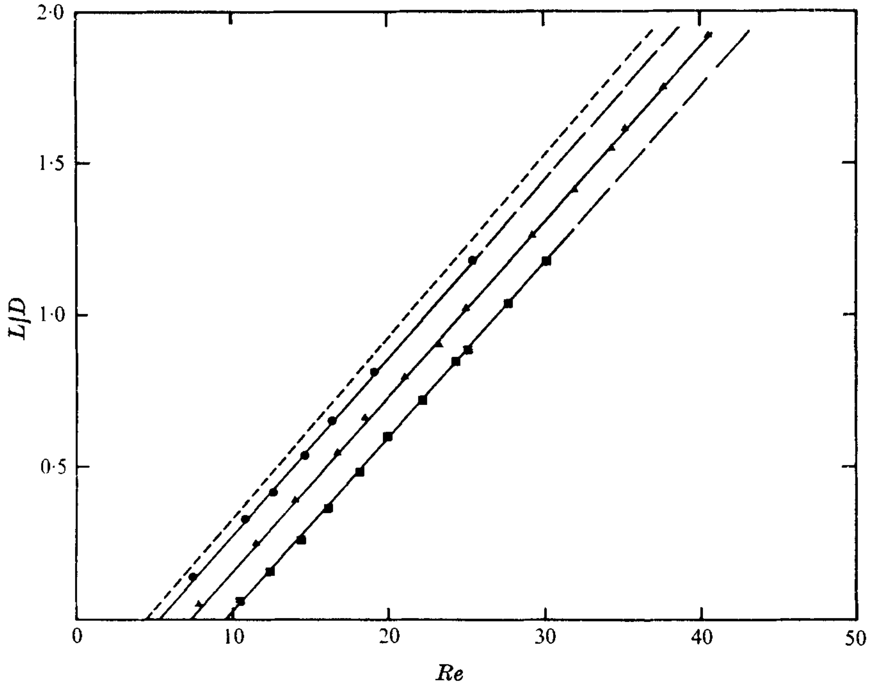

FIGURE 15. Length of the closed wake plotted atainst *Re*. ■, $\lambda = 0{\cdot}12$; ▲, $\lambda = 0{\cdot}07$; ●, $\lambda = 0{\cdot}024$; ------, $\lambda = 0$.

From our experimental curves, it appears that the evolution of $u_{\max}$ becomes linear rather rapidly after a certain limiting value Re_L which, in fact, is only slightly dependent on λ, for example, when $0 < \lambda < 0{\cdot}12$ we find $16 < Re_L < 17$. The linear parts of the curves have approximately a common slope $m_{u_{\max}} = 0{\cdot}0036$.

The position d of this maximum increases in direct proportion to *Re*, the straight-line slopes are the same for the three values of λ, consequently it is also the same for $\lambda = 0$; the common value is found to be $m_d \simeq 0{\cdot}024$.

From the investigation of the straight lines we can deduce with a fairly good accuracy the separation Reynolds number value Re_S at which the standing eddies appear.

The closed-wake geometrical-parameter determination

The main closed-wake geometrical parameters have been estimated, in particular, the length, maximum width, spread angle (often called 'separation angle') and the vortex-centre co-ordinates of the wake.

Closed wake length. Especially when it is small, the closed wake length is deduced with better accuracy from the curves of the velocity distribution than from a direct measurement on the photograph, something which does not seem to have been used by other authors. The wake length L is plotted against *Re* in figure 15 for the three studied values of λ. These curves show the effect of wall proximity on L. The dependence appears to be linear, for the range of *Re* considered, for all λ values ($0{\cdot}024 \leqslant \lambda \leqslant 0{\cdot}12$). In contrast to the results obtained by

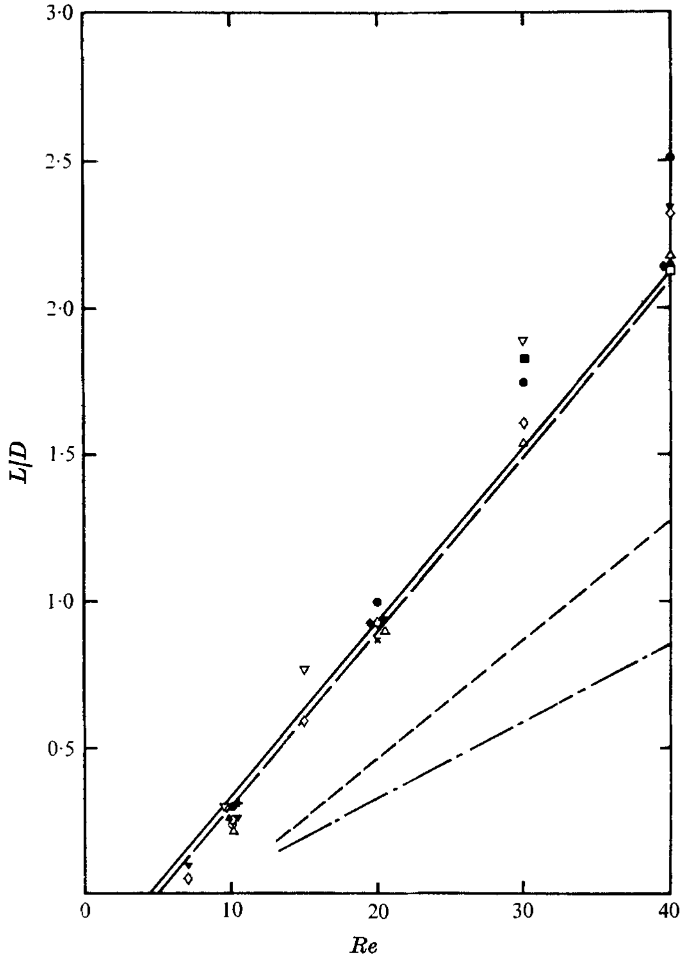

FIGURE 16. Length of the closed wake plotted against Re. Present data: ——, $\lambda = 0$. Experimental measurements: — —, $\lambda \leqslant 0{\cdot}03$, Taneda (1956*b*); - - - -, $\lambda = 0{\cdot}1$, — · —, $\lambda = 0{\cdot}02$, Grove *et al.* (1964). Numerical solutions: ×, Thom (1933); +, Allen & Southwell (1955); □, Apelt (1958); ●, Kawaguti & Jain (1966); ○, Underwood (1968); ◇, Takami & Keller (1969); ▽, Hamielec & Raal (1969); ■, Thoman & Szewczyk (1969); ▼, Dennis & Chang (1970); ▲, Collins & Dennis (1973); △, Nieuwstadt & Keller (1973); ◆, Ta Phoc Loc (1975).

Grove *et al.* (1964) and Acrivos *et al.* (1968) it can be seen that, within the accuracy of the measurements, the straight-line slope is the same for the three values of λ: $m_L \simeq 0{\cdot}058$. The quoted authors gave successively $m_L = 0{\cdot}070$, $0{\cdot}064$, $0{\cdot}041$, $0{\cdot}025$ when the 'blockage parameter' D/h_t (h_t is the tunnel height and D the cylinder diameter) is $0{\cdot}025$, $0{\cdot}050$, $0{\cdot}10$, $0{\cdot}20$. These values of D/h_t are then in the same range as our λ values. However, it is to be noticed that the tunnel cross-section of these experimenters is rectangular ($25{\cdot}4 \times 20{\cdot}32$ cm) and so, in their case but not in ours, there is a little difference between the length-to-diameter ratio of the cylinder and the D/h_t ratio. Further, because of their experimental conditions, the cylinder is not situated, as it is in our experiment, in an entirely uniform velocity flow. Also, we remark that the measurements have been made, as is often the case, with cylinders of smaller diameters than ours, with the result that there is significant imprecision in the reading, especially as the values were directly interpreted from the photographs. This appears clearly in figure 9: the bigger the cylinder, the better the definition of the flow pattern.

Moreover there are the experimental results of Taneda (1956*b*) and Nishioka & Sato (1974), from which we can deduce respectively $m_L \simeq 0{\cdot}060$ when $0{\cdot}005 < \lambda < 0{\cdot}03$ and $m_L \simeq 0{\cdot}070$ for the length-to-diameter ratio $D/h = 0{\cdot}15$ and $\lambda = 0{\cdot}05$.

We see that Taneda's result is very much in agreement with ours. On the other hand Nishioka & Sato's result is appreciably different. In this last case the velocity measurements are made with a hot-wire technique and with cylinders of diameters between 2·01 and 4·03 mm. The authors themselves point out their difficulties in measuring near the wall of the cylinder when Re is small. Consequently, these measurements have been made only for $Re > 65$ by artificially blocking the wake with a wall effect.

From the curves of L/D against Re, determined for different values of λ, we obtain by extrapolation the curve for $\lambda = 0$. This curve is plotted in figure 16, where we also report, for comparison, the many data in the literature which result, for the most part, from numerical investigations. With the drag coefficient, the wake length is in fact the most often calculated feature.

The intersection of the straight lines L/D *vs.* Re with the x axis give again values of the separation Reynolds number Re_S. We find, within the measurement accuracy, the same values we obtained by analysing the maximal velocity variation: so $Re_S = 4{\cdot}4$, $5{\cdot}2$, $7{\cdot}2$, $9{\cdot}6$ when $\lambda = 0$, $0{\cdot}024$, $0{\cdot}07$ and $0{\cdot}12$. But, because of our measurement technique, this last determination is more accurate.

These values of Re_S agree well with Taneda's result which gave $Re_S = 5$ when $0{\cdot}005 < \lambda < 0{\cdot}03$: so, by plotting the curve Re_S *vs.* λ we find $Re_S = 4{\cdot}5$ when $\lambda = 0{\cdot}005$ and $Re_S = 5{\cdot}4$ when $\lambda = 0{\cdot}03$. The accuracy of our measurements is sufficient to show the wall effects that the other authors considered as negligible.

The numerically calculated values of Re_S for unbounded flow ($\lambda = 0$) are, for the most part, perceptibly greater than those resulting from our experiments: generally they are between 5 and 7. The slope m_L is also greater. This confirms that the flow is particularly difficult to calculate within the closed wake.

However, it is to be noticed that from Ta Phoc Loc (1975), whose results are the most recent to our knowledge, we can deduce values of Re_S and m_L in very good agreement with ours.

Furthermore it seems from our analysis of the values of L and m_L that the most recent calculations are generally the most accurate, except for Apelt's results, which are very satisfactory despite being published some time ago. Also, it appears that, of the two calculation techniques described above, the one which uses the time-dependent equations seems to be less suited to the determination of steady-flow features (with the exception of the work of Collins & Dennis 1973).

On the other hand, every paper since 1969 which has been based on the equations of steady motion gives, when $Re = 20$, values of L similar to those we have deduced from our experiments with a discrepancy less than 4%; however,

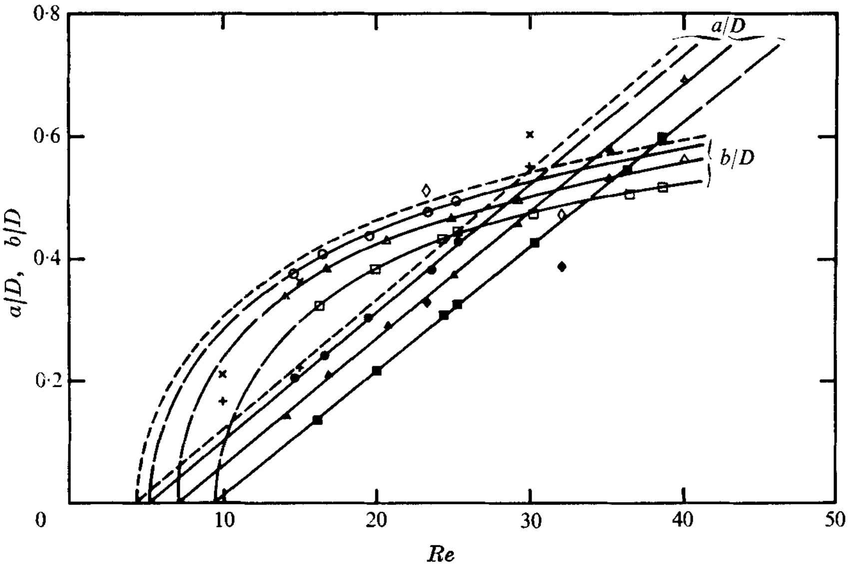

FIGURE 17. Co-ordinates of the vortex centre (a, b) plotted against Re. *Abscissa a*. Present data: ■, $\lambda = 0{\cdot}12$; ▲, $\lambda = 0{\cdot}07$; ●, $\lambda = 0{\cdot}024$; — — —, $\lambda = 0$. Numerical solutions: +, Hamielec & Raal (1969). Other experimental measurements: ◆, Grove *et al.* (1964). *Ordinate b*. Present data: □, $\lambda = 0{\cdot}12$; △, $\lambda = 0{\cdot}07$; ○, $\lambda = 0{\cdot}024$; ———, $\lambda = 0$. Numerical solutions: ×, Hamielec & Raal (1969). Other experimental measurements: ◇, Grove *et al.* (1964).

for $Re < 20$ the calculated lengths are, for the most part, perceptibly lower than those we obtain, whereas for $Re > 20$ they are for the most recent ones in good agreement with ours and rather appreciably higher for the former publications.

Finally, we remark that from the point of view of the infinite boundary conditions, the matching process with the irrotational flow or with Oseen flow seems to provide results closer to experimental results than the matching process with the uniform flow on the exterior boundary, even if this boundary is relatively distant from the obstacle

Vortex cores. The evolution of the 'vortex-core position' that we have located by the co-ordinates a, b is plotted against the Reynolds number for the three studied values of λ in figure 17. By extrapolation, we have drawn the curve corresponding to the unbounded field; we added Hamielec & Raal's (1969) calculated values, as well as the experimental results obtained by Grove *et al.*, who seem to be the only authors to give this information explicitly, but these values appear to be rather lacking in precision.

Our experiments show that the length a between the rear stagnation point and the line of the vortex centres changes in direct proportion to Re for the different values of λ; the slope m_a of the corresponding straight lines is about 0·021 for the three investigated cases.

Then, the ratio a/L between this length a and the wake length L is constant, its value being 0·36. Acrivos *et al.* made a similar remark and gave $a/L \simeq \frac{1}{3}$ for $D/h_t < 0{\cdot}1$ and $Re > 30$.

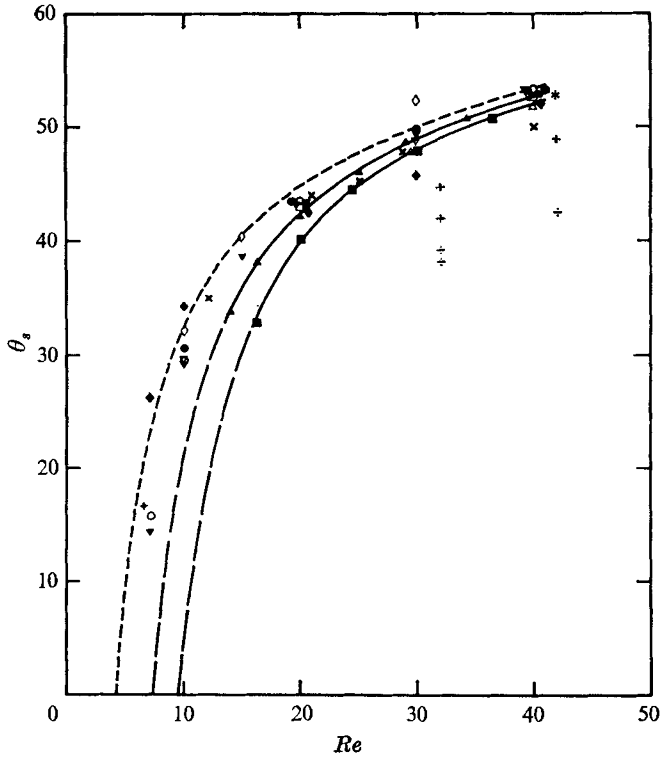

FIGURE 18. The separation angle plotted against *Re*. Present data: ■, $\lambda = 0{\cdot}12$; ▲, $\lambda = 0{\cdot}07$; ---, $\lambda = 0$. Numerical solutions: ◆, Dennis & Shimshoni (1965); ●, Kawaguti & Jain (1966); +, Underwood (1968); ▼, Takami & Keller (1969); ◇, Hamielec & Raal (1969); △, Thoman & Szewczyk (1969); ○, Dennis & Chang (1970); ▽, Nieuwstadt & Keller (1973); □, Ta Phoc Loc (1975). Experimental measurements: ×, Thom (1933); *, Taneda (1956*a*); ÷, with splitter plate, ·|·, no splitter plate, Grove *et al.* (1964).

On the other hand, contrary to the results of Grove *et al.* for $Re > 76$ and Nishioka & Sato (1974) for $Re > 65$, we establish that the maximum velocity point $P_{\max}$ is not located on the line that joins the vortex centres, but is rather appreciably downstream of this line: the ratio between the distances d and a is about 1·14 in all the studied cases.

Separation angle. The evolution of the separation angle θ_S with *Re* for $\lambda = 0{\cdot}07$ and 0·12 is presented in figure 18; the measurement of θ_S can be made with good accuracy for the values of *Re* close to Re_S only for sufficiently big cylinders; therefore we do not give any result for $\lambda = 0{\cdot}024$. In comparison with the previous feature evolution against the ratio λ, if we deduce, by a linear extrapolation, the θ_S value for $\lambda = 0$, we obtain a probably slightly higher value than the true one.

The values given in the literature for θ_S are rather dispersed, although some of them agree well with the results of our experiments. With regard to the other experimental values, it appears that the value given explicitly by Taneda, for $Re = 40$, is close to ours, but those of Grove *et al.* are different. This difference

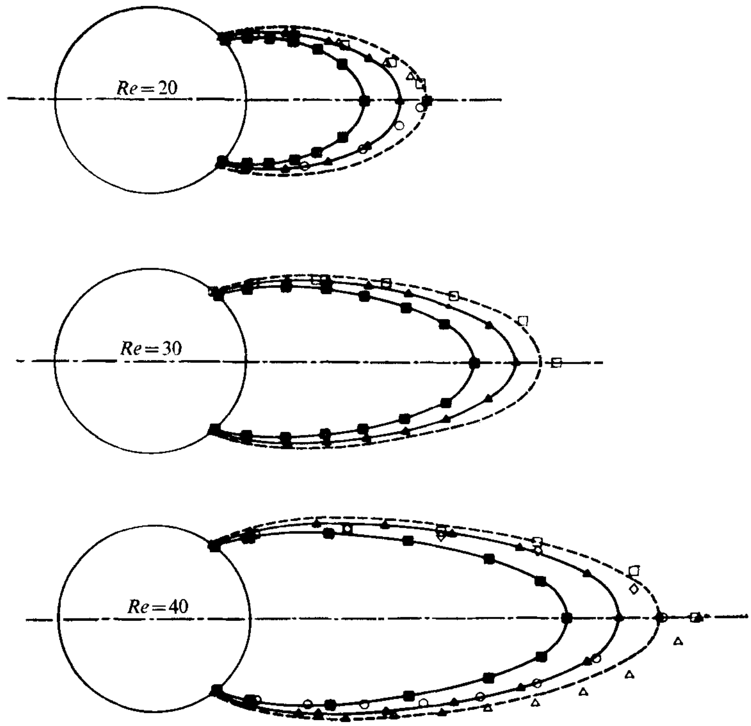

FIGURE 19. Shape of the wake boundary. Present study: ■, $\lambda = 0{\cdot}12$, $Re = 20$; ▲, $\lambda = 0{\cdot}07$, $Re = 21$; ---, $\lambda = 0$, $Re = 20$; ■, $\lambda = 0{\cdot}12$, $Re = 30{\cdot}2$; ▲, $\lambda = 0{\cdot}07$, $Re = 31$; ---, $\lambda = 0$, $Re = 30$; ■, $\lambda = 0{\cdot}12$, $Re = 38{\cdot}6$; ▲, $\lambda = 0{\cdot}07$, $Re = 40{\cdot}5$; ---, $\lambda = 0$, $Re = 40$. Theoretical data: ◇, Apelt (1958); □, Takami & Keller (1969); △, Dennis & Chang (1970); ○, Ta Phoc Loc (1975).

might be explained by the fact that these authors deduced their results from a method which used a heated cylinder; thus they probably obtained a different flow from the one investigated here.

For $Re > 20$ and $\lambda = 0$ (i.e. no wall effect) the curve of θ_S against Re becomes almost a straight line when plotted on a logarithmic scale. This agrees with the results of, for instance, Kawaguti & Jain (1966), Takami & Keller (1969), Son & Hanratty (1969) and Pruppacher, Le Clair & Hamielec (1970). This tendency is also verified for a confined flow but the Reynolds numbers must be as much higher as the diameter ratio is larger.

Attached-wake boundary. The attached-wake boundary is drawn in figure 19, for $Re \simeq 20$, 30, 40 and $\lambda = 0$, $0{\cdot}07$, $0{\cdot}12$.

For unbounded flow ($\lambda = 0$), the wake boundary is determined from the experiments as follows: for any value of λ, let y be the ordinate of a wake boundary point and let δ $(= x - R)$ be its abscissa measured from the rear stagnation point. Introducing a reduced abscissa $\eta = \delta/\delta_1$, and reduced ordinate $\mathscr{L} = y/y_1$, where δ_1 and y_1 are typical dimensions of the wake, for example the wake length and half the distance between its vortex cores, we find that the boundary ($\mathscr{L}$ *vs.* η) is independent of λ and so distributions for different values of λ merge into a single

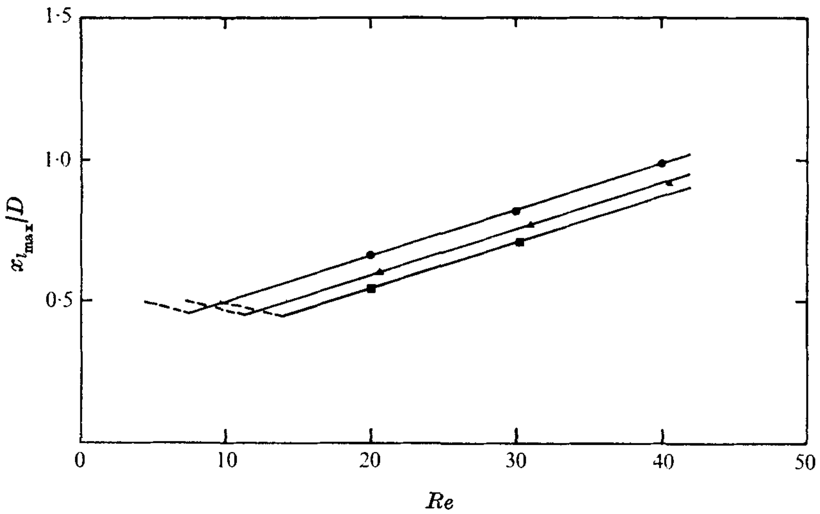

FIGURE 20. Abscissa of the maximum width plotted against *Re*.
■, $\lambda = 0{\cdot}12$; ▲, $\lambda = 0{\cdot}07$; ●, $\lambda = 0$; ---, x_S.

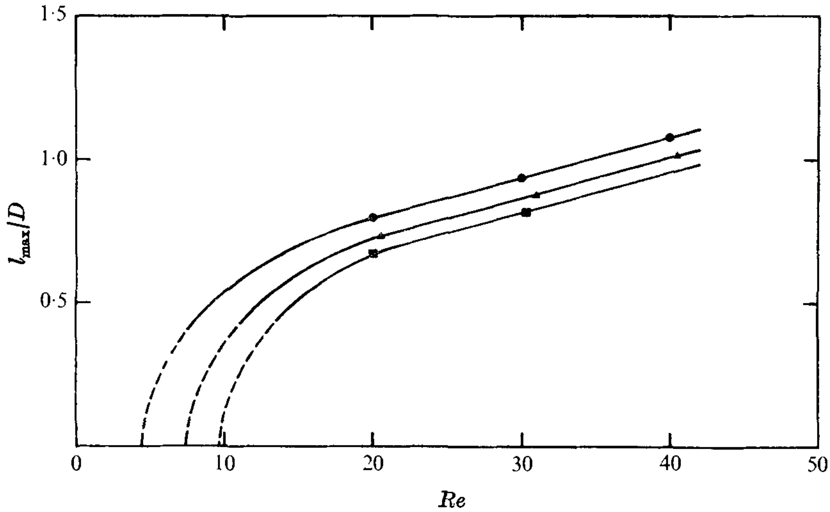

FIGURE 21. The maximum width plotted against *Re*.
■, $\lambda = 0{\cdot}12$; ▲, $\lambda = 0{\cdot}07$; ●, $\lambda = 0$; ---, l_S.

curve. The wake length and the core separation being known from extrapolation when $\lambda = 0$, we can deduce the corresponding wake boundary. The shape evolution againt Reynolds number and against the diameter ratio λ appears clearly in figure 19.

In particular, it is to be remarked that the wake width takes a maximum value (l_{max}) within a section which moves away from the cylinder when *Re* increases; this section is located by its abscissa ($x_{l_{max}}$), measured from the centre of the right section of the cylinder (figure 5).

On figure 19 we have plotted some data that result from numerical calculations; we have kept only the most recent ones.

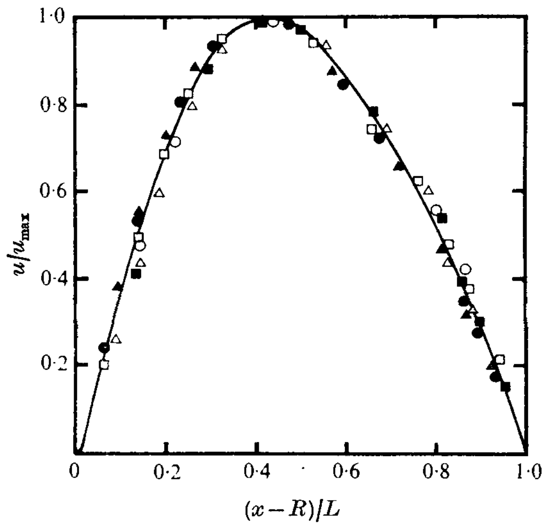

FIGURE 22. Velocity similarity on the rear flow axis in the closed wake. $\lambda = 0{\cdot}12$: ○, $Re = 14{\cdot}6$; △, $Re = 25{\cdot}1$; □, $Re = 29{\cdot}5$. $\lambda = 0{\cdot}07$: ■, $Re = 21{\cdot}2$; ●, $Re = 29{\cdot}5$; ▲, $Re = 40{\cdot}5$.

It is seen that, although the values given by Ta Phoc Loc are generally very close to our experimental values for the length and the separation angle, the wake shape that this author deduces from his calculations is too angular towards its rear extremity; the general wake shapes obtained by Apelt, Takami & Keller and Dennis & Chang are rather closer to the experimental boundaries that we have deduced for the unbounded flow ($\lambda = 0$). However, the maximum width calculated by the various authors is, for a given value of Re, always lower than ours. From this point of view, the Dennis & Chang calculations give the best results, particularly when $Re = 40$, when we see that the calculated and experimental boundaries coincide, up to a diameter length downstream of the cylinder.

Maximum wake width. Figures 20 and 21 show the variation of the maximum width l_{max} and the abscissa $x_{l_{max}}$ of the corresponding section against Re. We find again the fact that we have pointed out before: the typical abscissae of the attached wake increase in direct proportion to Re.

Analysis of experimental results shows also that this maximum width does not always exist: near the separation Reynolds number, immediately after the attached wake appears, its width regularly decreases from l_s, its value on the cylinder, down to zero at its rear extremity. It was necessary, to find this maximum again, to give to the outline of the wake an imaginary prolongation within the right section of the cylinder, as Van Dyke (1964) proposed for the sphere. That is the reason why we have completed our figure by drawing the curves that give the width l_s and abscissa x_s of the corresponding section; the intersection between the straight lines x_s and $x_{l_{max}}$ provides the limit Re_l for the existence of a maximum. Furthermore, it is seen that from this value of Re_l the curves of l_s and l_{max} are matched in a continuous way.

For the two cases studied ($\lambda = 0{\cdot}12$ and $\lambda = 0{\cdot}07$) and also for the extrapolated

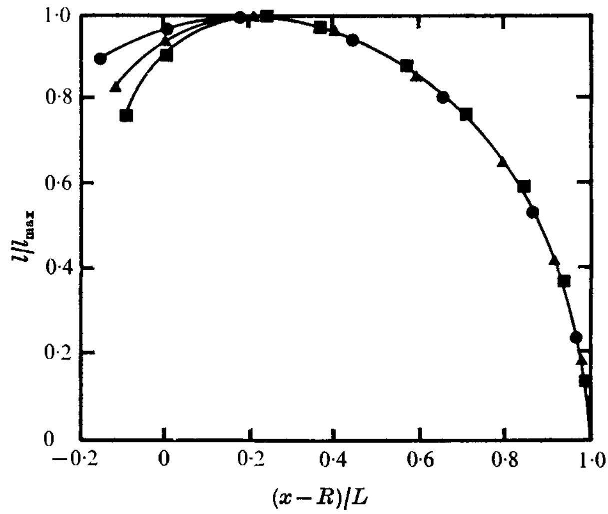

FIGURE 23. Similarity of the closed-wake shape: ●, Re = 20; ▲, Re = 30; ■, Re = 40.

λ \ Re ...		10	15	20	30	40
0·12	L	0·03	0·31	0·60	1·17	1·75
	a	0·01	0·12	0·22	0·42	0·62
	b	0·12	0·31	0·39	0·47	0·52
	$x_{l_{max}}$	—	—	0·55	0·71	0·86
	l_{max}	—	—	0·68	0·83	0·96
	θ_S	—	30·0°	40·0°	48·0°	52·0°
0·07		0·16	0·45	0·73	1·31	1·89
		0·06	0·17	0·27	0·48	0·68
		0·24	0·36	0·42	0·50	0·56
		—	—	0·59	0·75	0·92
		—	—	0·73	0·88	1·01
		21·0°	36·0°	42·3°	49·0°	52·8°
0·024		0·28	0·58	0·87	1·46	2·04
		0·11	0·21	0·31	0·52	0·73
		0·29	0·39	0·45	0·53	0·58
0		0·34	0·63	0·93	1·53	2·13
		0·12	0·23	0·33	0·55	0·76
		0·31	0·40	0·47	0·54	0·59
		—	—	0·66	0·83	0·99
		—	—	0·80	0·95	1·08
		32·5°	40·5°	44·8°	50·1°	53·5°

TABLE 2. Numerical values of the closed-wake geometrical parameters deduced from our experiments.

Author(s) \ *Re*		10	15	20	30	40
Thom (1933)	L	—	—	0·87	—	—
	θ_S	—	—	40°	—	—
Kawaguti (1953)		—	—	—	—	1·6177*
		—	—	—	—	52·5°
Allen & Southwell (1955)		0·31	—	—	—	—
		34·8°	—	—	—	—
Taneda (1956*a, b*)		0·3	0·6	0·9	1·5	2·1*
		—	—	—	—	53°*
Apelt (1958)		—	—	—	—	2·135*
		—	—	—	—	50°
Dennis & Shimshoni (1965)		0·56	—	1·06	1·16	0·94
		34·8°	—	42·8°	46°	52·3°
Hirota & Miyakoda (1965)		—	—	—	—	1·46
		—	—	—	—	38°
Kawaguti & Jain (1966)		0·30	—	1·00	1·75	2·515*
		30·8°	—	43·8°	50°	53·7°
Underwood (1968)		0·24	—	—	—	—
		30°	—	—	—	—
Ingham (1968)	L	—	—	—	—	1·6
Takami & Keller (1969)		0·25*	0·589*	0·935*	1·611*	2·325*
		29·3°*	38·7°*	43·65°*	49·6°*	53·55°*
Hamielec & Raal (1969)	L	0·303*	0·77*	—	1·89*	—
	θ_S	32·4°*	40·6°*	—	52·7°*	—
	a	0·169*	0·223*	—	0·547*	—
	b	0·211*	0·361*	—	0·602*	—
Son & Hanratty (1969)		—	—	—	—	2·515*
		—	—	—	—	53·9°*
Jain & Rao (1969)		—	—	—	—	2·65*
		—	—	—	—	54·2°*
Thoman & Szewczyk (1969)		—	—	—	1·83*	—
		—	—	—	48°	52°
Dennis & Chang (1970)		0·265*	—	0·94*	—	2·345*
		29·6°	—	43·7°	—	53·8°
Nieuwstadt & Keller (1973)		0·217*	—	0·893*	1·543*	2·179*
		27·96°*	—	43·37°*	49·39°*	53·34°*
Collins & Dennis (1973)		0·26*	—	—	—	2·15*
		29·6°*	—	—	—	53·6°*
Ta Phoc Loc (1975)		—	—	0·93	—	2·14
		—	—	43°	—	53°

TABLE 3. Numerical values of some geometrical parameters of the closed wake given by different authors for a flow of infinite extent.

case ($\lambda = 0$), the straight lines x_s and $x_{l_{\max}}$ intersect, within the accuracy of the measurement, at the same value of x ($x/D \simeq 0{\cdot}45$), corresponding to Re_l being, respectively, about 13·9, 11·3, 7·4. For these values of Re_l, the wake boundary then leaves the obstacle wall in a direction parallel to the flow.

The slope of the straight lines giving the abscissa of the maximum width section against Re is about 0·016.

It is then possible to deduce from it that the ratios between the abscissa of the maximum width section and the abscissae of the cores of the maximum velocity section are respectively 0·76 and 0·67: consequently the maximum width section is located rather in front of the cores and therefore in a more forward position than the maximum velocity section.

We get that, when $20 < Re < 40$, the ratio between the length that separates the cores and the maximum width of the wake is nearly constant, for any values of Re and λ; then we have $0{\cdot}55 < b/l_{\max} < 0{\cdot}58$, while Acrivos *et al.* found $b/l_{\max} \simeq \frac{3}{5}$ when $D/h_t < 0{\cdot}1$ and $Re > 30$.

Wake similarity

The different properties that we have pointed out, concerning the variation of the parameters and of the velocities within the attached wake, seem to show that there is a similarity in the evolution of these various features.

That is shown in figures 22 and 23, where we have plotted the ratios $u/u_{\max}$ and $l/l_{\max}$ against η ($= (x-R)/L$). It is seen that the results, for different values of Re and of λ, respectively merge in a single curve.

However with regard to $l/l_{\max}$, this property is not verified near the cylinder wall; it is so only for $x-R \geqslant 0{\cdot}2L$.

In table 2 we have recapitulated the numerical values of the geometrical parameters of the attached wake that are deduced from our experiments. In table 3 we present various numerical information given by the authors either explicitly (indicated by an asterisk) or by means of curves.†

Range of wake stability: determination of the critical Reynolds number

We tried to determine the value of the Reynolds number giving the upper limit of wake stability ('critical Reynolds number'); we analyse its evolution against the wall effect, i.e. against the diameter ratio λ.

In particular, a systematic study of the variation of wake shape and of the core position against Re (near Re_c) shows, when $\lambda = 0{\cdot}07$, that the wake boundary begins to warp towards is rear end and that the distances between each of the cores and the rear stagnation point F become different: this last phenomenon is easier to measure than the boundary deformation, which is why we keep this last test to detect the 'birth' of the instability; that does not seem to be used by other authors.

Let a^- and a^+ be the lengths that separate the nearest and the farthest vortex centres from the plane of the rear stagnation point. We compare their evolution against Re with the prolongation of the curve *a vs. Re* that we have obtained in

† The values read on the curves of the cited authors can be rather lacking in precision as the corresponding diagrams are sometimes published on a very small scale.

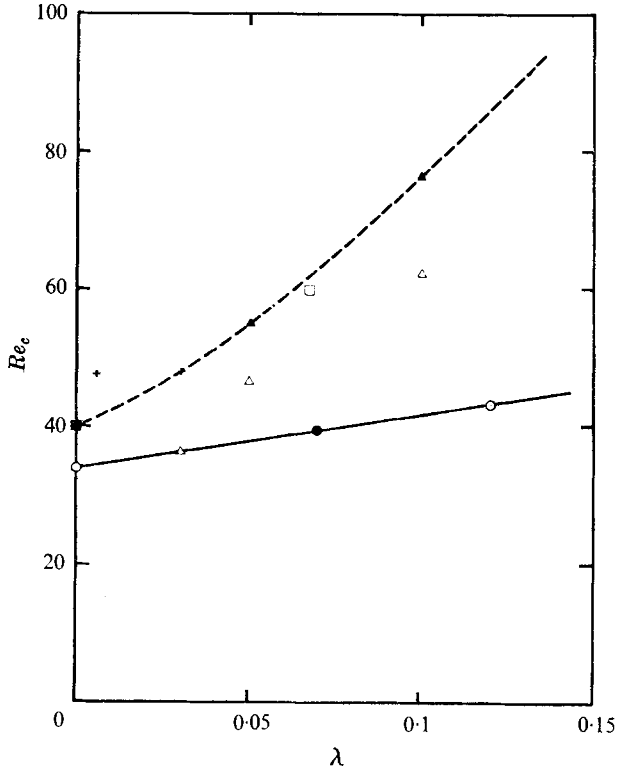

FIGURE 24. Critical Reynolds number against the diameter ratio λ. Present data: ●, $\lambda = 0{\cdot}07$; —○—, $l_{max} = 1$. Experimental measurements: +, Dupin & Teissie-Solier (1928); △, Thom (1933); □, Homann (1936); ■, Kovasznay & Roskho (1949–1954); –▲– –, Shair *et al.* (1963).

the case of symmetrical flow. It appears that the length a^- begins to decrease abruptly from some value of *Re* and then becomes stable at about $a/D = 0{\cdot}55$, while the length a^+ changes in fairly random way; according to the inevitable small variations in the experimental conditions either core can be nearest the cylinder.

Investigation of all the results (about twenty studied photographs when $39 < Re < 44$) gives as the value of the critical Reynolds number $Re_c \simeq 39{\cdot}5$ when $\lambda = 0{\cdot}07$.

We notice that, for this value of Re_c, the maximum wake width is nearly equal to the length of the cylinder diameter. To verify this result it will be interesting to do again this work for other values of the diameter ratios λ but this requires a rather important modification of our apparatus; we are thinking of attempting this study in the future.

If, as a temporary assumption, we suppose this property is the same for other values of λ, we can deduce the Re_c values from the curves l_{max} *vs.* *Re*, and then find, respectively, $Re_c = 43$, 39·5, 36, 34 when $\lambda = 0{\cdot}12$, 0·07, 0·024 and 0.

This evolution is shown in figure 24 and a comparison is made with the results of Dupin & Tessie-Solier (1928), Thom (1933), Homann (1936), Kovasznay

(1949), Roshko (1954) and Shair *et al.* (1963). When $0{\cdot}005 < \lambda < 0{\cdot}03$, Taneda remarks that the wake 'trail' begins to oscillate at $Re = 30$, while he perceives the vortex asymmetry only at $Re = 45$. This comparison of the different results shows, as we have furthermore pointed out during experimental investigation, that the accurate location of the vortex cores allows us to show an asymmetry so faint that it will not appear by means of a global investigation of the photographs. It is the reason why the critical Reynolds numbers that we have found are consistently smaller than the values usually given in the literature.

4. Conclusion

The fine technique of visualization that we have perfected allows us to give the detailed features of the hydrodynamic field for Reynolds numbers ranging from the 'separation number' (for which the flow separates and the attached closed wake appears) to the 'critical number' (from which it becomes asymmetrical and unstable).

We have measured the velocities on the flow axis, determined the geometrical parameters of the attached wake and shown their evolution against Re and against the diameter ratio λ.

This systematic investigation allows us, in particular, to deduce the flow features for the unbounded case ($\lambda = 0$) and thus to make a comparison with the existent numerical results, allowing us to formulate some critical comments about certain points of the different calculation techniques.

On the other hand, we have shown general properties concerning the attached wake structure, in particular the following.

(i) The wake length and all the abscissae that characterize it and that we have studied (abscissae of the cores, of the maximum velocity point, of the maximum width section) increase linearly with increasing Reynolds number and analogously whatever the wall effect may be (for $0 \leqslant \lambda \leqslant 0{\cdot}12$ the slopes are identical); such is not the case for the ordinates, except, perhaps, for the greatest values of the studied Reynolds numbers.

(ii) The variation of the velocities along the returning flow axis, like that of the longitudinal attached wake features, with the Reynolds number and with the diameter ratio λ is similar; this allows us to regroup certain results in a main curve. The similarity is also verified for the transverse features, but outside the region very close to the cylinder.

Finally, we have determined the limiting values of the Reynolds number for which a stable attached wake exists and shown their greater or lesser sensibility to the wall effect.

REFERENCES

Acrivos, A., Leal, L. G., Snowden, D. D. & Pan, F. 1968 Further experiments on steady separated flows past bluff objects. *J. Fluid Mech.* **34**, 25.

Allen, D. N. de G. & Southwell, R. V. 1955 Relaxation methods applied to determine the motion, in two dimensions, of a viscous fluid past a fixed cylinder. *Quart. J. Mech. Appl. Math.* **8**, 129.

APELT, C. J. 1958 The steady flow of a viscous fluid past a circular cylinder at Reynolds numbers 40 and 44. *Aero. Res. Counc. R. & M.* no. 3175.

BOUROT, J. M., COUTANCEAU, M. & MOREAU, J. J. 1962 Sur l'étude théorique et expérimentale des phénomènes d'orientation présentés par une suspension lamellaire dans un écoulement de Stokes. *C.R. Acad. Sci.* **255**, 1377.

BOUROT, J. M. & MOREAU, J. J. 1949 Sur les zones d'inégale luminosité observées dans certaines visualisations d'écoulements. *C.R. Acad. Sci.* **228**, 1567.

CHARTIER, C. 1937 Chronophotogrammétrie plane et stéréoscopique. *Ministère de l'Air, Publ. Sci. Tech.* no. 114.

COLLINS, W. M. & DENNIS, S. C. R. 1973 Flow past an impulsively started circular cylinder. *J. Fluid Mech.* **60**, 105.

COUTANCEAU, M. 1962 Etude théorique et expérimentale de l'orientation des particules lamellaires mises en suspension dans un écoulement méridien. Thèse de Doctorat de Troisième Cycle.

COUTANCEAU, M. 1968 Mouvement d'une sphère dans l'axe d'un cylindre contenant un liquide visqueux. *J. Méc.* **7**, 49.

COUTANCEAU, M. 1971 Contribution à l'étude théorique et expérimentale de l'écoulement autour d'une sphère qui se déplace dans l'axe d'un cylindre, à faible nombre de Reynolds ou en régime irrotationnel. Thèse de Doctorat d'Etat.

COUTANCEAU, M. 1972 Sur l'étude expérimentale de l'écoulement engendré par une sphère qui se déplace dans l'axe d'un cylindre au-delà du régime de Stokes. *C.R. Acad. Sci.* A **274**, 853.

DENNIS, S. C. R. & CHANG, G. Z. 1970 Numerical solutions for steady flow past a circular cylinder at Reynolds numbers up to 100. *J. Fluid Mech.* **42**, 471.

DENNIS, S. C. R. & SHIMSHONI, M. 1965 The steady flow of a viscous fluid past a circular cylinder. *Aero. Res. Counc. Current Papers*, no. 797.

DIMOPOULOS, H. G. & HANRATTY, T. J. 1968 Velocity gradients at the wall for flow around a cylinder for Reynolds numbers between 60 and 360. *J. Fluid Mech.* **33**, 303.

DUPIN, P. & TEISSIE-SOLIER, M. 1928 *Rev. Gén. Elec.* **24**, 53.

FAGE, A. 1934 Photographs of fluid flow revealed with an ultramicroscope. *Proc. Roy. Soc.* **144**, 381.

GROVE, A. S., SHAIR, F. H., PETERSEN, E. E. & ACRIVOS, A. 1964 An experimental investigation of the steady separated flow past a circular cylinder. *J. Fluid Mech.* **19**, 60.

HAMIELEC, A. E. & RAAL, J. D. 1969 Numerical studies of viscous flow around circular cylinders. *Phys. Fluids*, **12**, 11.

HIROTA, I. & MIYAKODA, K. 1965 Numerical solution of Kármán vortex street behind a circular cylinder. *J. Met. Soc. Japan*, **43**, 30.

HOMANN, F. 1936 Der Einfluss grosser Zähigkeit bei der Strömung um den Zylinder und um die Kugel. *Z. angew. Math. Mech.* **16**, 153.

IMAI, I. 1951 On the asymptotic behaviour of viscous fluid flow at a great distance from a cylindrical body, with special reference to Filon's paradox. *Proc. Roy. Soc.* A **208**, 487.

INGHAM, D. B. 1968 Note on the numerical solution for unsteady viscous flow past a circular cylinder. *J. Fluid Mech.* **31**, 815.

JAIN, P. C. & RAO, K. S. 1969 Numerical solution of unsteady viscous incompressible fluid flow past a circular cylinder. *Phys. Fluids Suppl.* **12**, II 57.

KAPLUN, S. 1967 Low Reynolds number flow past a circular cylinder. *J. Math. Mech.* **6**, 595.

KAWAGUTI, M. 1953 Numerical solution of the Navier–Stokes equations for the flow around a circular cylinder at Reynolds number 40. *J. Phys. Soc. Japan*, **8**, 747.

KAWAGUTI, M. & JAIN, P. C. 1966 Numerical study of a viscous fluid flow past a circular cylinder. *J. Phys. Soc. Japan*, **21**, 2055.

KOVASZNAY, L. S. G. 1949 Hot-wire investigation of the wake behind cylinders at low Reynolds numbers. *Proc. Roy. Soc.* A **198**, 174.

LAGERSTROM, P. A. & COLE, J. D. 1955 Examples illustrating expansion procedures for the Navier–Stokes equations. *J. Rat. Mech. Anal.* **4**, 817.

NIEUWSTADT, F. & KELLER, H. B. 1973 Viscous flow past circular cylinders. *Computers & Fluids*, **1**, 59.

NISHIOKA, M. 1973 Hot-wire investigation of the steady laminar wake behind a circular cylinder. *Bull. Univ. Osaka Prefecture*, **21**, 205.

NISHIOKA, M. & SATO, H. 1974 Measurements of velocity distributions in the wake of a circular cylinder at low Reynolds numbers. *J. Fluid Mech.* **65**, 97.

NISI, H. & PORTER, A. W. 1923 On eddies in air. *Phil. Mag.* **46** (6), 754.

PAYARD, M. & COUTANCEAU, M. 1974 Sur l'étude expérimentale de la naissance et de l'évolution du tourbillon attaché à l'arrière d'une sphère qui se déplace, à vitesse uniforme, dans un fluide visqueux. *C.R. Acad. Sci.* B **278**, 369.

PROUDMANN, I. & PEARSON, J. R. A. 1957 Expansion at small Reynolds numbers for the flow past a sphere and a circular cylinder. *J. Fluid Mech.* **2**, 237.

PRUPPACHER, H. R., LE CLAIR, B. P. & HAMIELEC, A. E. 1970 Some relation between drag and flow pattern of viscous flow past a sphere and a cylinder at low and intermediate Reynolds numbers. *J. Fluid Mech.* **44**, 781.

ROSHKO, A. 1954 *N.A.C.A. Rep.* no. 1191.

SHAIR, F. H., GROVE, A. S., PETERSEN, E. E. & ACRIVOS, A. 1963 The effect of confining walls on the stability of the steady wake behind a circular cylinder. *J. Fluid Mech.* **17**, 546.

SON, J. S. & HANRATTY, T. J. 1969 Numerical solution for the flow around a cylinder at Reynolds numbers of 40, 200 and 500. *J. Fluid Mech.* **35**, 369

TAKAISI, Y. 1969 Numerical studies of a viscous liquid past a circular cylinder. *Phys. Fluids Suppl.* **12**, II 86.

TAKAMI, H. & KELLER, H. B. 1969 Steady two-dimensional viscous flow of an incompressible fluid past a circular cylinder. *Phys. Fluids Suppl.* **12**, II 51.

TANEDA, S. 1956*a* Experimental investigation of the wakes behind cylinders and plates at low Reynolds numbers. *J. Phys. Soc. Japan*, **11**, 302.

TANEDA, S. 1956*b* Experimental investigation of the wakes behind a sphere at low Reynolds numbers. *J. Phys. Soc. Japan*, **11**, 1104.

TANEDA, S. 1964 Experimental investigation of the wall-effect on a cylindrical obstacle moving in a viscous fluid at low Reynolds numbers. *J. Phys. Soc. Japan*, **19**, 1024.

TANEDA, S. 1965 Experimental investigation of vortex streets. *J. Phys. Soc. Japan*, **20**, 1714.

TA PHOC LOC 1975 Etude numérique de l'écoulement d'un fluide visqueux incompressible autour d'un cylindre fixe ou en rotation. Effet Magnus. *J. Méc.* **14**, 109.

THOM, A. 1928 *Aero. Res. Counc. R. & M.* no. 1194.

THOM, A. 1933 The flow past circular cylinders at low speeds. *Proc. Roy. Soc.* A **141**, 651.

THOMAN, D. C. & SZEWCZYK, A. A. 1969 Time-dependent viscous flow over a circular cylinder. *Phys. Fluids Suppl.* **12**, II 76.

TRITTON, D. J. 1959 Experiments on the flow past a circular cylinder at low Reynolds numbers. *J. Fluid Mech.* **6**, 547.

UNDERWOOD, R. L. 1968 Calculation of incompressible flow past a circular cylinder at moderate Reynolds numbers. *J. Fluid Mech.* **37**, 95.

VAN DYKE, M. 1964 Perturbation methods in fluid mechanics. *Appl. Math. Mech.* **8**, 149.

ZANDBERGEN, P. J. 1971 The viscous flow around a circular cylinder. *Lecture Notes in Physics*, vol. 8, p. 144. Springer.

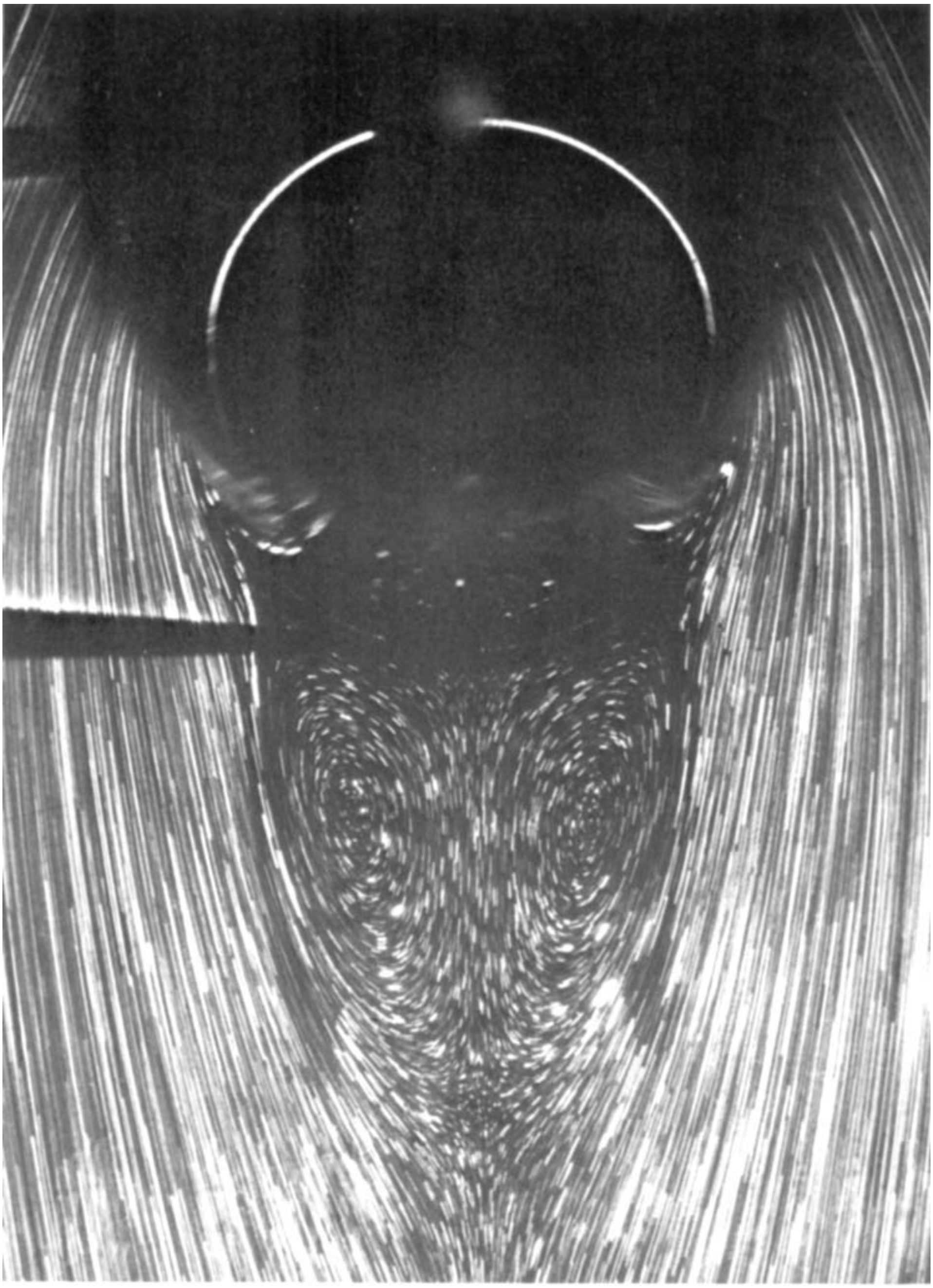

FIGURE 4. $Re = 24{\cdot}3$, $\lambda = 0{\cdot}12$.

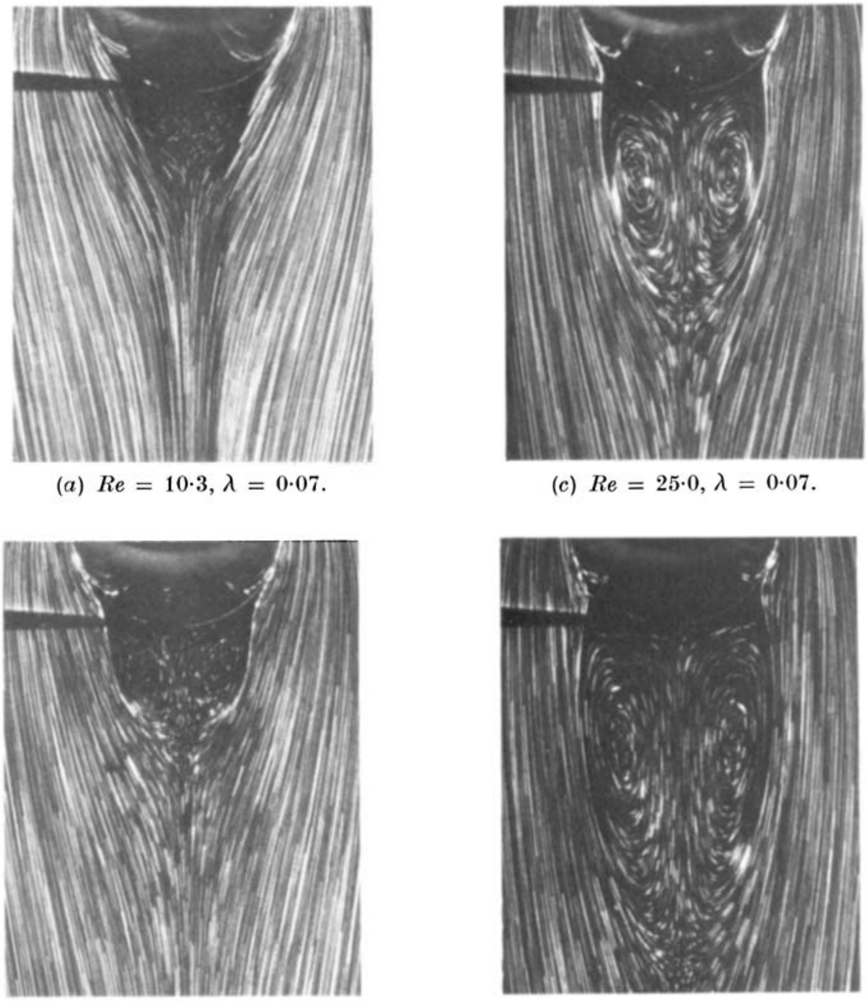

(*a*) $Re = 10{\cdot}3$, $\lambda = 0{\cdot}07$.

(*b*) $Re = 16{\cdot}6$, $\lambda = 0{\cdot}07$.

(*c*) $Re = 25{\cdot}0$, $\lambda = 0{\cdot}07$.

(*d*) $Re = 35{\cdot}2$, $\lambda = 0{\cdot}07$.

FIGURE 6

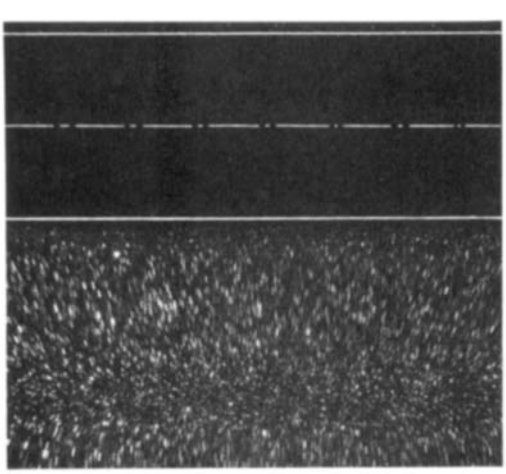

FIGURE 7. $Re = 25{\cdot}6$, $\lambda = 0{\cdot}12$, $h/D \simeq 8$.

FIGURE 8. $Re = 40{\cdot}3$, $\lambda = 0{\cdot}07$.

(*a*) $Re = 19{\cdot}9$, $\lambda = 0{\cdot}12$.

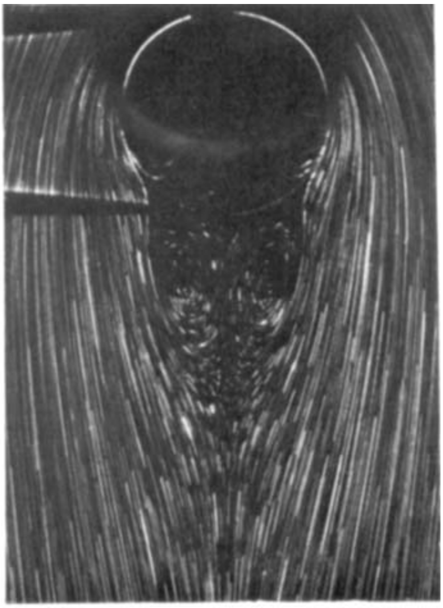

(*b*) $Re = 20{\cdot}6$, $\lambda = 0{\cdot}07$.

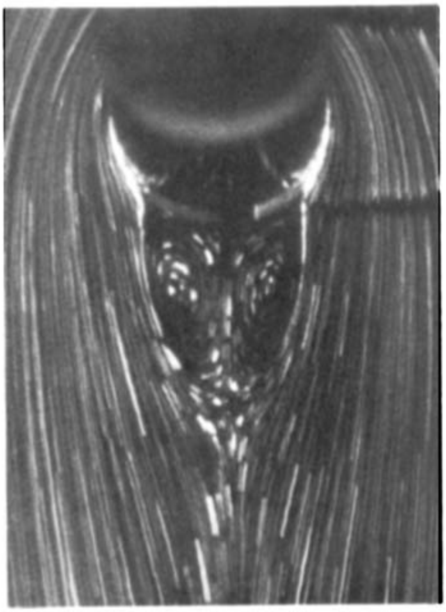

(*c*) $Re = 20{\cdot}1$, $\lambda = 0{\cdot}024$.

FIGURE 9